JOURNAL OF GEOPHYSICAL RESEARCH, VOL. 100, NO. B7, PAGES 9817–9830, JUNE 10, 1995

A P wave velocity model of Earth's core

Xiaodong Song[1] and Don V. Helmberger
Seismological Laboratory, California Institute of Technology, Pasadena

Abstract. Present Earth core models derived from the retrieval of global Earth structure are based on absolute travel times, mostly from the International Seismological Centre (ISC), and/or free-oscillation eigenfrequencies. Many core phase data are left out of these constructions, e.g., *PKP* differential travel times, amplitude ratios, and waveforms. This study is an attempt to utilize this additional information to construct a model of core P wave velocity which is consistent with the different types of core phase data available. In conjunction with our waveform modeling we used 150 differential time measurements and 87 amplitude ratio measurements, which were the highest-quality observations chosen from a large population of Global Digital Seismograph Network (GDSN) records. As a result of fitting these various data sets, a one-dimensional P wave velocity model of the core, PREM2, is proposed. This model, modified from the Preliminary Reference Earth Model (PREM) (Dziewonski and Anderson, 1981), shows a better fit to the combined data set than any of the existing core models. Major features of the model include a sharp velocity discontinuity at the inner core boundary (ICB), with a large jump (0.78 km/s), and a low velocity gradient at the base of the fluid core. The velocity is nearly constant over the lower 100 km of the outer core. The model features a depth-dependent Q_α structure in the inner core such that a constant t^* for the inner core fits the amplitude ratios and waveforms of short-period waves moderately well. This means the top of the inner core is more attenuating than the deeper part of the inner core. In addition, the P velocity in the lowermost mantle is reduced from that of PREM as a baseline adjustment for the observed separations of the *DF* and *AB* branches of *PKP* at large distances.

Introduction

One-dimensional velocity models continue to play important roles both in seismology and in Earth physics and chemistry. The former is needed as a reference in locating new events and as a comparison to anomalous events. The latter is typically used in studying mineralogy in terms of pressure and temperature, especially the complexities caused by the boundary layers at the core-mantle boundary and at the inner core-outer core boundary.

In this paper we present a spherically symmetric one-dimensional (1-D) P wave velocity model of the Earth's core and lowermost mantle along with a simple P wave attenuation model of the inner core from *PKP* waveforms and differential times. We use the Preliminary Reference Earth Model (PREM) [*Dziewonski and Anderson*, 1981] as the starting model and derive a consistent 1-D model that satisfies, simultaneously, differential travel times, amplitude ratios, and waveforms of all branches of the *PKP* phases for the data we analyzed. As a first geometric ray arrival after the core shadow zone, *PKP* is observed throughout the distance range of around 120° to 180°, thus providing a unique data set to study the structure of Earth's deep interior. Figure 1a shows the ray paths of various branches of *PKP* phases. The D'' region is highlighted to indicate the complex structure presently known. Figure 1b shows the travel time curve of these *PKP* phases for a surface focus: *PKP-AB*, *PKP-BC*, *PKIKP* (or *PKP-DF*) and *PKiKP* (or *PKP-CD*). The dashed line beyond the *C*-cusp is the diffracted wave *PKP-*C_{diff} which propagates along the inner core boundary (ICB). It provides an important data set for constraining the structure above the ICB, which will be discussed later. The distance range is limited to 130° to 165° in this study.

This work is motivated by that fact that present Earth core models, derived in the framework of global Earth structure, are based on absolute travel times (mostly from the International Seismological Centre (ISC)) and/or free-oscillation eigenfrequencies. The addition of differential travel time, amplitude, and waveform information proves crucial in testing and refining detailed structure of the Earth's core, particularly near the inner core boundary and the core-mantle boundary. Recent studies suggest that there is ample room

[1] Now at Lamont-Doherty Earth Observatory of Columbia University, Palisades, New York.

Paper number 94JB03135.
0148-0227/95/94JB-03135$05.00

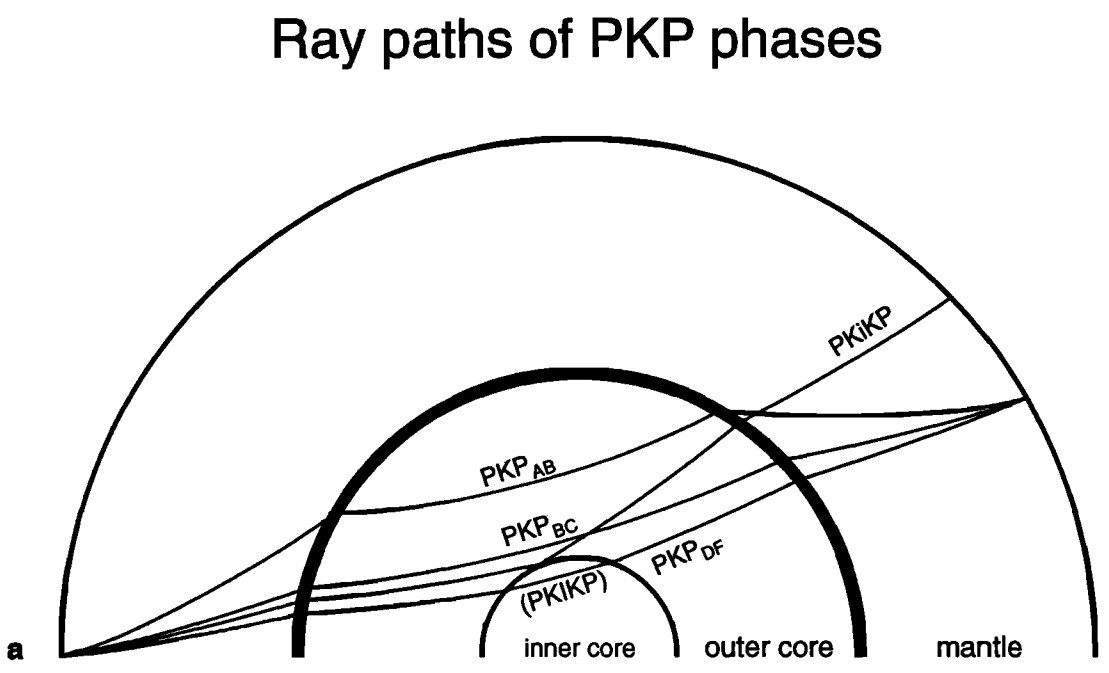

Figure 1. (a) Ray paths of *PKP* phases used in this study. (b) Travel time curves of *PKP* triplications for the Earth's core model of this study (PREM2) for a surface focus. The dashed line *PKP-C*$_{diff}$ is the diffraction propagating along the inner core boundary.

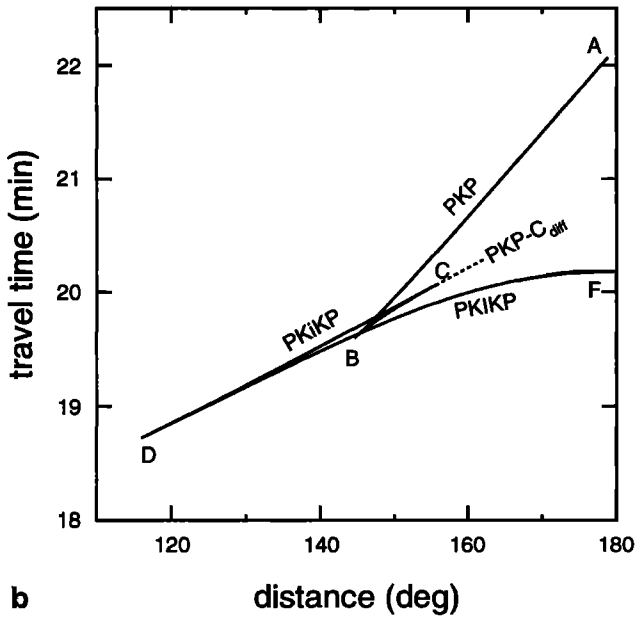

Figure 1. (continued)

to improve model parameters, e.g., a regional waveform study of *PKP* phases by *Song and Helmberger* [1992].

Our data contain a mixed set of digital and analog records consisting of both short- and long-period seismograms from the Global Digital Seismograph Network (GDSN), the World-Wide Standard Seismograph Network (WWSSN) and Long Range Seismic Measurements (LRSM) network. Figure 2 shows the ray coverage of the data used. The dashed lines indicate GDSN paths for which *BC*/*DF* amplitude ratios are derived. The solid lines are GDSN paths for which differential *PKP* travel times are picked, which are a subset of paths used for defining the amplitude ratios. The dotted lines show ray paths of WWSSN record sections for two events from Java and Tonga. The ray coverage is somewhat restricted because of data quality and the distribution of earthquakes and stations. The data consist of (1) differential time measurements from short-period GDSN seismograms: 52 for $BC - DF$, 50 for $AB - DF$, 48 for $AB - BC$; (2) 87 *BC*/*DF* amplitude ratio measurements from short-period GDSN seismograms; (3) 16 long-period WWSSN seismograms, 20 short-period GDSN and WWSSN seismograms, and seven short-period LRSM records of *Song and Helmberger* [1992]. For the differential travel times, only those with cross-correlation coefficients of waveforms larger than 0.5 were used as by *Song and Helmberger* [1993a]. The seismograms used to determine the amplitude ratios were selected with high signal-to-noise ratios. So were the waveforms used in our forward modeling but the availability of a number of good stations for a given event was the major restriction. Thus it should be realized that although the data quality is high, our modeling results could be biased by the limited data set.

Figure 3 shows our model PREM2 in comparison with the starting model PREM. A variety of the observations, as mentioned above, were used not only as a way for checking the self-consistency of the model but also as an effective way to constrain the model due to the different sensitivities of the data to the velocities in various regions. This study pieces together our previous results near the ICB [*Song and Helmberger*, 1992] and and the *D*″ [*Song and Helmberger*, 1993a] with modifications to fit the average of a larger data set. The

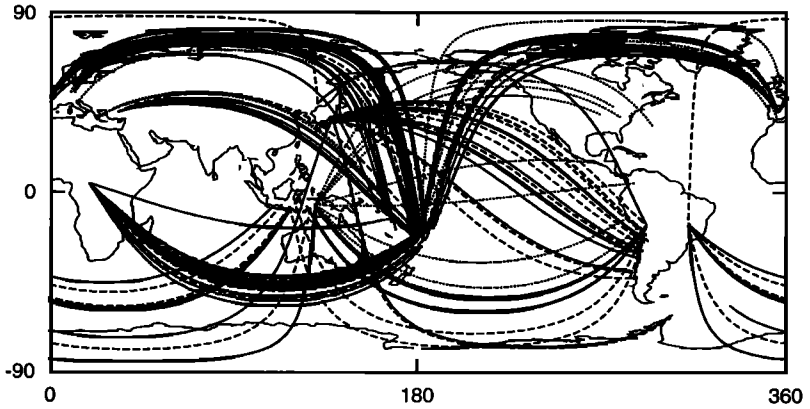

Figure 2. Ray coverage of the data used in this study. Dashed lines are Global Digital Seismograph Network (GDSN) paths for which *BC/DF* amplitude ratios are picked. Solid lines are GDSN paths for which differential *PKP* travel times are picked. Dotted lines show ray paths of World-Wide Standard Seismograph Network (WWSSN) record sections for two events from Java and Tonga. The data used include 150 different time measurements, 87 amplitude ratio measurements, and 43 waveform records.

major features of PREM2 include the following. (1) It has a large velocity jump at the inner core boundary (0.78 km/s). Short-period *PKIKP* and *PKiKP* waveforms from 130° to 140° are very sensitive to the jump at the boundary [*Cummins and Johnson*, 1988; *Song and Helmberger*, 1992]. This number is the same as in the model PMNA by *Song and Helmberger* [1992], which fits a short-period LRSM record section in the distances of 130° to 136° from an Indonesia event to North America, sampling the ICB under northeastern Pacific, extremely well. This increased velocity jump also fits better to the short-period WWSSN records in the distances of 132° to 139° from a Java event to North America stations, sampling a similar region of the ICB, than PREM (see Figures 12 and 13 and discussion later). (2) The model has a near-zero gradient for the bottom 150 km of the fluid core. Travel times and amplitudes of *PKP-BC* and *PKP-*C_{diff} are very sensitive to the velocity gradient; thus $BC - DF$ (or *PKP-*$C_{diff}-DF$) and *BC/DF* (or *PKP-*C_{diff}/DF) provide strong constraints. (3) It has a nearly constant t^*=0.35 s for the inner core attenuation, which means that the attenuation decreases as the depth increases into the inner core. Assuming this velocity model, the attenuation at the top of the inner

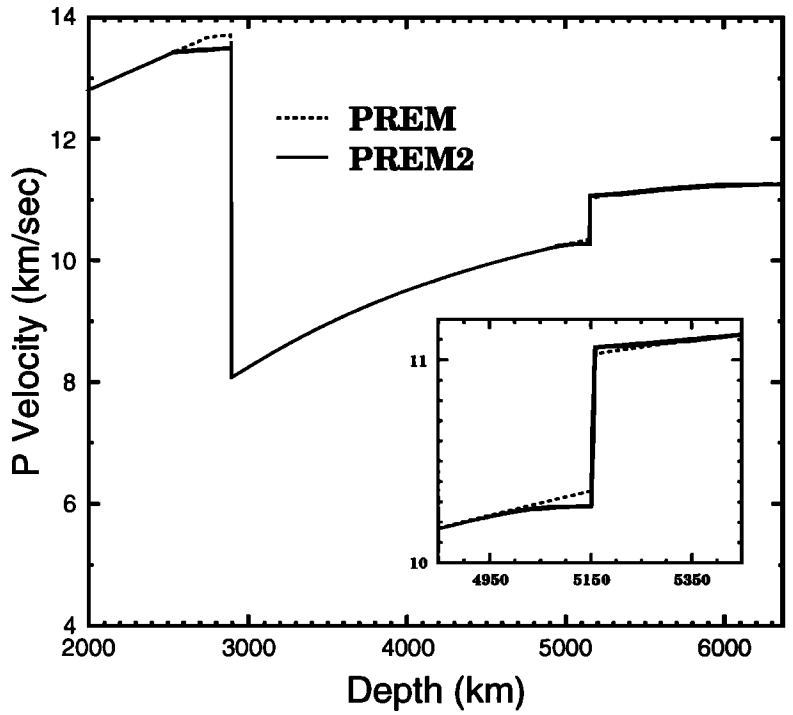

Figure 3. *P* wave velocity model PREM2 of this study (solid), which is modified from PREM (dashed).

core was estimated from the *BC/DF* amplitude ratios in the range of 148° to 158°. A constant t^*=0.35 s fits the observations reasonably well. Another feature of PREM2 is that it has an average velocity lower than PREM in the lowermost mantle. The velocity is reduced by about 1.5% in the lowermost 350 km of the mantle to fit the average of $AB - DF$ observations. $AB - DF$ differential travel times are very sensitive to the velocity in this region and have been used to explore possible lateral variations in D'' [*Song and Helmberger*, 1993a]. This feature can be viewed as an effective baseline shift rather than a definitive structure due to regional variations, which is discussed further in the concluding section. Shear wave velocity and density of PREM are assumed in this study due to the poor sensitivity to them by the *PKP* data. Although this assumption does not significantly affect our results on the *P* wave velocity structure, our estimation of Q_α in the inner core is subject to modification if other values of shear wave and density are assumed for the inner core. The discussion on trade-off between shear wave and Q_α near the ICB by *Cummins and Johnson* [1988] serves as an excellent guide to what the problem should lead to.

Figure 4 shows our preferred model along with some other global models. The zero line is the reference model PREM. All the other models are plotted with respect to PREM to highlight the differences near the core-mantle boundary (CMB) and the inner core boundary (ICB). The models include PEM [*Dziewonski et al.*, 1975], derived from observations of eigenfrequencies, surface wave dispersion data, and body wave travel times, IASP91 [*Kennett and Engdahl*, 1991], and SP6 [*Morelli and Dziewonski*, 1993], derived from body wave travel times from ISC. Note that IASP91 uses the PEM core model. The radii of the inner core and the outer core are not the same in these models, the largest difference being the inner core radius of SP6, which is smaller than PREM (or PREM2) by 6.5 km.

In the following, we present the details of the model development and give justifications for the above conclusions and discuss limitations of any 1-D model in describing the Earth. One immediate problem is the anisotropy of the inner core. There is increasing evidence that the inner core is anisotropic with the direction parallel to the spin axis being fast [*Shearer et al.*, 1991; *Creager*, 1992; *Tromp*, 1993; *Song and Helmberger*, 1993b]. Our recent systematic search for data that sample paths nearly parallel to the spin axis confirms that these polar paths are indeed anomalous. Waves that travel parallel to the spin axis in the upper part of the inner core are on average 3% faster than waves that travel perpendicular to it. However, this anisotropic effect is apparent only for polar paths with ray angles from the spin axis less than about 40°. Because of limited earthquake and station distributions, these polar paths account for only a small portion of *PKP* recording. For nonpolar paths, which include all the paths in this study, this effect is within the scatter of the data. Thus in this study we are averaging only nonpolar paths for the inner core.

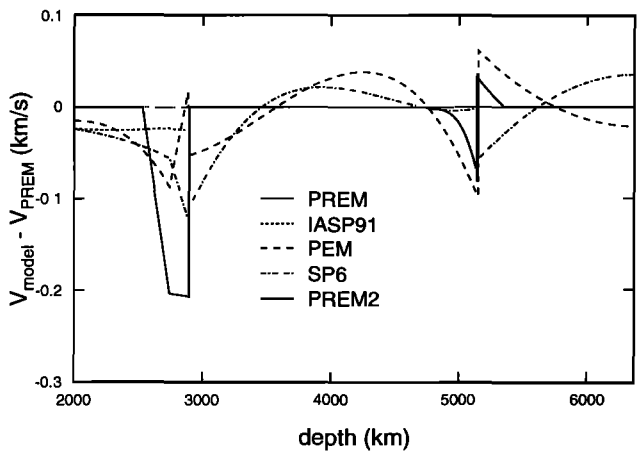

Figure 4. Models used in this study: PEM [*Dziewonski et al.*, 1975], PREM [*Dziewonski and Anderson*, 1981], IASP91 [*Kennett and Engdahl*, 1991], SP6 [*Morelli and Dziewonski*, 1993], and our model, PREM2. The models are plotted relative to PREM.

Modeling Results

Our strategy in modeling the data is basically a trial-and-error procedure. We first determine a preliminary model that satisfies the travel time differentials between the various branches of *PKP*. Then, we generate synthetics for this model and compare them with the observed amplitude ratios and waveforms, especially at key distances where the *BC* branch becomes diffracted. This process is reiterated until satisfactory fits are found to the different types of *PKP* data available.

Like any other forward modeling approach, finding a model by trial and error that fits all observations can be tedious and time-consuming. To aid our modeling practice, an interactive model design software is developed, which allows us to manipulate velocity profiles easily. Particularly, Bézier curves are used to model smoothly varying velocity profiles. Bézier curves are widely used in computer graphics and computer-aided designs (CAD) because only a few points are needed to model a complex shape and the tangent vectors at end points can be easily modified by the control point or points in between [e.g., *Mortenson*, 1985]. Thus, they are very useful in fine-tuning the velocity gradient at the base of the outer core. Table 1 shows model parameters of PREM2 in the form of polynomials. The current model represents the best fitting model of dozens of test models. The lowermost mantle and the top of the outer core are linear fits. The Bézier curve for the velocity profile at the base of the outer core is approximated as a third-order polynomial. Note that the second-order discontinuities at the depth of 4749.5 km in the outer core and the depth of 5361 km in the inner core result from our choices of Bézier curve fitting (first-order continuous) and linear fitting (zero-order continuous), respectively. They have no physical significance.

Differential Travel Times

The differential travel time results are summarized in Figures 5, 6, and 7. The solid dots are the observed

Table 1. P Wave Velocity Model of Earth's Core (PREM2) Proposed in This Study

Depth, km	Radius, km	V_p, km/s (x=Radius/a, a=6371 km)
2531.0-2891.0	3840.0-3480.0	$14.2743 - 1.3998x$
2891.0-4749.5	3480.0-1621.5	$11.0487 - 4.0362x + 4.8023x^2 - 13.5732x^3$
4749.5-5149.5	1621.5-1221.5	$4.0354 + 82.008x - 347.769x^2 + 468.786x^3$
5149.5-5361.0	1221.5-1010.0	$11.3041 - 1.2730x$
5361.0-6371.0	1010.0-0.0	$11.2622 - 6.3640x^2$

The polynomial for the depth range (4749.5-5149.5 km) just above the inner core boundary is an approxiamtion to the velocities expressed by a Bézier curve for the region.

differential travel times, corrected to a surface focus for comparisons. The error bars show ± one standard deviation about the the averages of the data in 2° intervals, expressing 68% of probability for a Gaussian error distribution. The various lines show the predictions for a surface focus of different models as indicated in the legend boxes. Note that the diffractions beyond the C-cusp, $PKP\text{-}C_{diff}$, are shown as long-dashed lines for all the models in Figure 5 and 7. The travel times of these diffractions are calculated from synthetic seismograms. Also, note these times for PREM and SP6 are not plotted at distances larger than 156° because it becomes difficult to determine the differential times from the weak diffracted arrivals for these two models. Predictions of our new model PREM2 are shown by solid lines, which fit the average of the observations fairly well for all three data sets.

Figure 5 shows the comparisons of the observations and predictions of various models for $BC - DF$. As mentioned earlier, $BC - DF$ is useful in constraining the structure near the ICB. The predictions of PREM are smaller by about 0.3 s than the data average at distances larger than 152°, whereas the predictions of IASP91 and PEM models are larger than the data by about 0.6 s. The latter two models agree because the IASP91 model adopted the core model of PEM. The predictions of model SP6 are smaller than the data by 0.5 s to 0.8 s. The smaller core radius and lower velocity at the top of the inner core of the model slows down DF, thus decreasing the $BC - DF$ differential times. The predictions of PREM2 and the model by *Souriau and Poupinet* [1991] (hereafter denoted as S-P91) fit the average of the data very well at larger distances. The S-P91 model is based on PREM but with a reduced velocity gradient at the base of the outer core to fit BC and $PKP\text{-}C_{diff}$ residuals at distances larger than 152°. Thus both the PREM2 and S-P91 models have a similar flat velocity structure in the bottom 150 km of the outer core. This velocity reduction effectively slows down BC relative to DF at larger distances, thus increasing $BC - DF$ differentials. However, the fits of S-P91 to $BC - DF$ times at distances smaller than 150° are less satisfactory. Some compensation is needed at the top of the inner core to speed up DF when BC is not affected by the reduced velocity at smaller distances. Predictions of our previous model PMNA of the

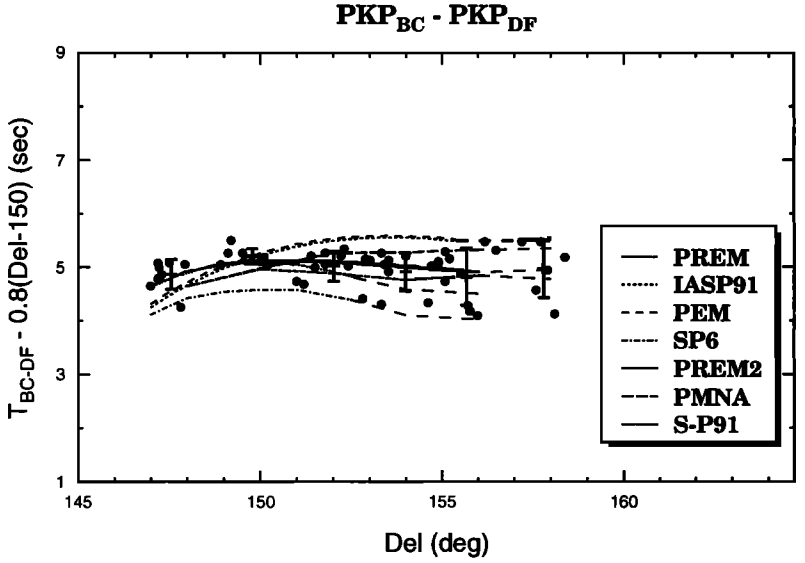

Figure 5. Comparisons of GDSN $BC - DF$ observations with predictions of various Earth models for a surface focus. Long-dashed lines indicate $PKP\text{-}C_{diff}$. Compared with the data from 150° to 158°, predictions of PREM are too small, while predictions of IASP91 and PEM are too big. SP6 underpredicts the data average by more than 0.5 s. Both PREM2 and the model from *Souriau and Poupinet* [1991] (denoted as S-P91), which have a similar flat velocity gradient at the bottom of the outer core, fit significantly better than the other models.

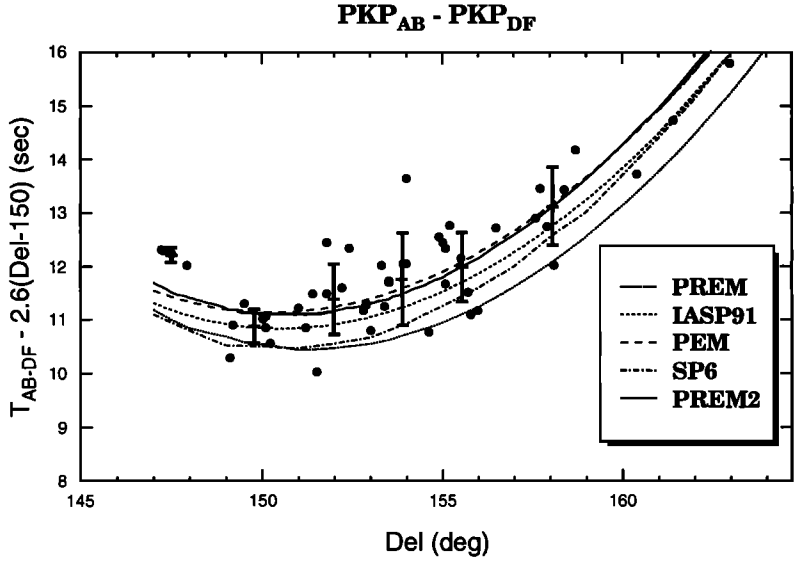

Figure 6. Comparisons of GDSN $AB - DF$ observations with predictions of various Earth models. Long-dashed lines indicate $PKP\text{-}C_{diff}$.

ICB do not fit the observed $BC - DF$ times very well. They fall on the upper bounds of the data at distances larger than 152° and lower bounds at distances less than 150°. A broad velocity reduction in the model relative to PREM effectively slows down BC relative to DF at larger distances, while a velocity reduction at the top of the inner core slows down DF at smaller distances.

Figure 6 shows the comparisons of the $AB - DF$ observations and predictions of various models. This data set is sensitive to the velocity in the lowermost mantle as well as the top of the inner core. We see that predictions of IASP91, PEM, and PREM2 all fit the average of the data. SP6 underpredicts the average of the data by more than 0.5 s while PREM underpredicts it by nearly 1 s. Because AB has a much greater incident angle than DF at the lowermost mantle, the velocity reduction in PREM2 in this region effectively slows down AB and thus significantly increases the $AB - DF$ travel time. A simple linear structure is used in PREM2's lowermost mantle because the detailed velocity structure in this region, such as the discontinuity depth and velocity gradient, is not constrained by the $AB - DF$ differential times [*Song and Helmberger*, 1993a]. On the other hand, the velocity structure both in the lowermost mantle and the top of the inner core contributes to the differences between the PEM and PREM predictions. The velocity at the top of the inner core in PEM is significantly higher than in PREM which speeds up DF, while the velocity in the lowermost mantle is significantly lower in PEM than in PREM which slows down AB. Similar

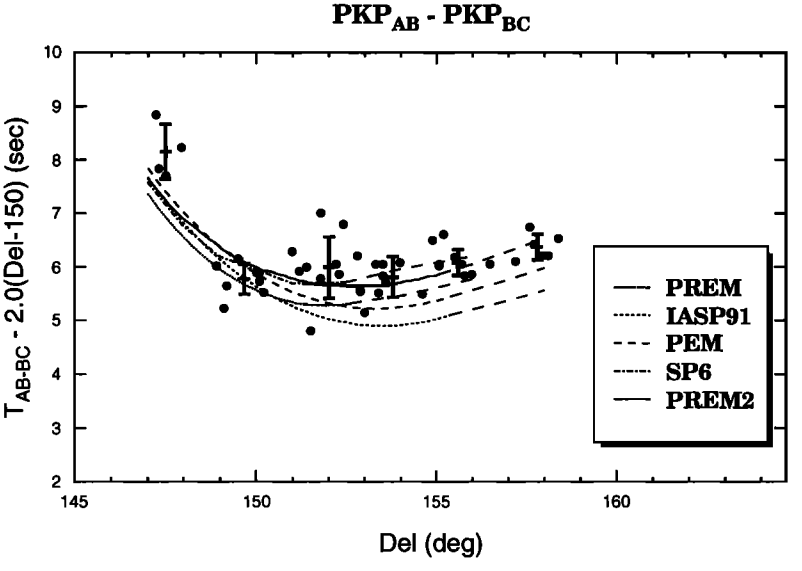

Figure 7. Comparisons of GDSN $AB - BC$ observations with predictions of various Earth models. Long-dashed lines indicate $PKP\text{-}C_{diff}$.

reasoning can be applied to the comparison of IASP91 and PREM since IASP91 and PEM have the same core model. The only exception is that the velocity structure in the lowermost mantle in IASP91 is closer to PREM than PEM. Although the negative gradient structure of SP6 in the lowermost mantle slows down AB considerably, this effect on $AB - DF$ is partly offset by the slow velocity in the uppermost inner core.

Figure 7 displays the $AB - BC$ comparisons. This data set is sensitive to the velocity structure at the lowermost mantle and at the base of the outer core. It is impossible to judge which one of these regions contributes more to these data because of the trade-off between them. This trade-off is made clear by comparing the predictions of PEM and PREM. The differences in $AB - BC$ from both models are much smaller than in $AB - DF$ because the velocity decrease in the lowermost mantle in PEM is compensated by the velocity decrease at the base of the outer core. Furthermore, the two curves cross each other at about 152° because BC from PEM is slowed down considerably at larger distances when it approaches the ICB.

Amplitude Ratios

Figures 8a and 8b show the amplitude ratios of BC/DF from the GDSN short-period records and synthetic predictions of PREM2. The observed amplitude ratios (shown by dots) are divided into two groups according

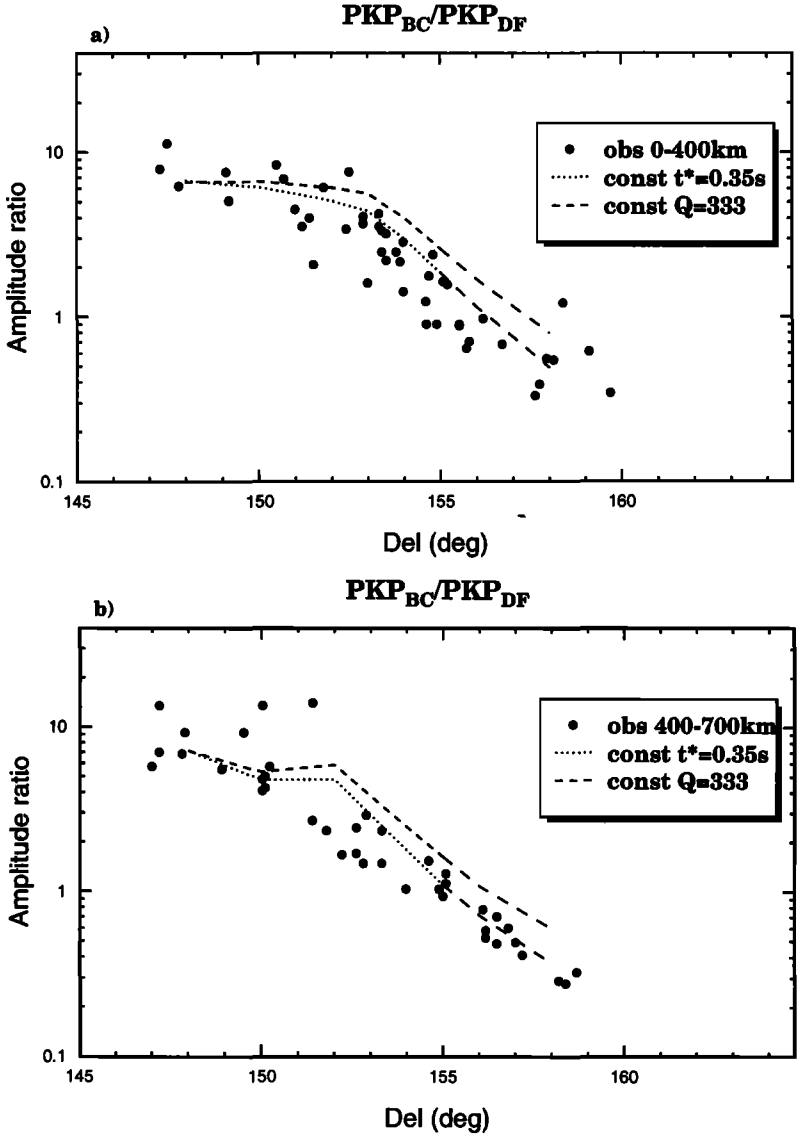

Figure 8. Comparisons of GDSN BC/DF observations with synthetic predictions of the PREM2 model. Long-dashed lines indicate $PKP\text{-}C_{diff}$. (a) The event depths are shallower than 400 km. The synthetics are for a source depth of 200 km; (b) The event depths are greater than 400 km. The synthetics are for a source depth of 600 km. A constant t^*=0.35 s and a constant Q_α in the inner core were applied to the DF branch of the synthetics. Although there is room for improvement, the constant t^* model provides fair fits to the the amplitude ratios. A uniform Q_α model is unlikely to explain these amplitude ratios.

to focal depths, shallower than 400 km and deeper than 400 km, to distinguish slight variations in amplitude ratios from synthetic predictions at different depths. While travel times primarily depend on velocity structure, amplitude ratios depend on attenuation structure as well as velocity. Assuming a velocity structure of the lowermost outer core and the inner core, it is possible to invert for the depth dependence of Q_α at the top of the inner core from BC/DF amplitude ratios. A simple experiment is shown in Figures 8a and 8b where a constant $t^*$and a uniform Q_α are applied, using the velocity model from PREM2. The dotted lines show the synthetic amplitude ratios of BC/DF with a constant t^*=0.35 s. The dashed lines show the synthetic amplitude ratios of BC/DF for a constant Q_α=333, which was chosen to fit the observed ratios around 148°. Clearly, a uniform Q_α model is unlikely to to explain the amplitude ratios. The synthetic BC/DF ratio is more than 50% larger than the average observed ratio at 156°. Adjustment of the Q_α value to fit observations at large distances would significantly mismatch observations at smaller distances. The fits from the constant t^* model are good for the deep events (Figure 8b) and marginal for the shallow events (Figure 8a). This value of t^*=0.35 s is in close agreement with our previous estimate of t^*=0.4 s for the very top of the inner core from waveform modeling of LRSM short-period records at distances from 130° to 136° [*Song and Helmberger*, 1992].

Since t^* is the time integral of Q_α^{-1} along the ray path, a constant t^* for the inner core suggests that the attenuation decreases with depth in the inner core. Similar results have been suggested by *Doornbos* [1974] and *Choy and Cormier* [1983]. However, *Cormier* [1981] favors a depth-independent Q_α model, although the scatter of the data does not rule out a model in which Q_α increases with depth [*Choy and Cormier*, 1983]. Recently, *Bhattacharyya et al.* [1993] measured t^* values for the inner core from short-period *PKP-BC* and *PKP-DF* waveforms from the same GDSN data set as in this study. They conclude that the scatter of the t^* measurement cannot resolve any depth or frequency dependence of Q_α in the inner core and thus neither dependence is required. However, the study covers a limited depth range of the inner core (150-320 km from distance range of 146.4° to 153.9°) so that the depth effect of Q_α may not be obvious. Moreover, the analysis may be flawed by not including any propagation effect of the *DF* and *BC* waves. Also, the measurements of t^* by cross-correlation of *DF* and *BC* phases may be unstable; it was pointed out by *Bhattacharyya et al.* [1993] that there is often a small range of t^* values which give nearly the same value of cross-correlation coefficient as for the best fitting case.

The observed amplitude ratios of BC/AB and DF/AB are less useful for our purpose. They show much larger scatter than BC/DF ratios due to larger influence of heterogeneity of the lowermost mantle and/or radiation patterns on AB relative to DF or BC. The scatter of DF/AB amplitude ratios has been used to map the heterogeneity of the lowermost mantle by *Sacks et al.* [1979].

Waveform Studies

Ultimately, of course, we should be able to model the waveforms of these core phases. The advantage of using waveforms is that waveforms contain much more information than mere travel times and amplitudes as demonstrated in numerous modeling studies. Since variations of waveforms are commonly found for different sampling paths, it is not practical to model every detail of the seismograms. Rather, we strive to examine the adequacy or inadequacy of using a spherically symmetric 1-D model to represent the Earth's core structure by comparing the waveforms of the data and the synthetics.

Figure 9 shows comparison of GDSN short-period records from earthquakes at depths of around 150 km with generalized ray synthetics for PREM2. The synthetics are computed at a focal depth of 150 km for all the traces except the trace at 160°, which is computed at 250 km. Amplitudes are normalized relative to *BC* at distances smaller than 154° and relative to *DF* at distances larger than 154°. A constant t^*=0.35 s has been applied to the synthetics. The synthetics generally resemble the observations, especially the decaying amplitudes of $PKP\text{-}C_{diff}$ at distances larger than 154°.

While the observations displayed in Figure 9 proved useful in determining relative timing and in amplitude control, they are less useful in waveform modeling. This shortcoming is caused by the lack of source control since every observation is from a different event with its unique source time function. Thus the more dense network of analog stations, such as WWSSN and LRSM, has distinct advantages in waveform comparisons because the same source can be used and a record section constructed.

Figure 10 shows examples of the fits of synthetics for PREM2 (dashed) to long-period WWSSN records (solid). The event is from West Tonga on March 17, 1966, with a focal depth of 627 km. The source time function used is a simple trapezoid of (0.5 s, 1.8 s, 1.5 s). The observed waveforms are shifted to line up with the *DF* arrivals of the synthetics. Both data and synthetics are normalized to peak-to-peak amplitudes. We see excellent fits throughout the distance ranges except for the two stations PTO and TOL. The differential travel times of $AB - DF$ for these two stations are anomalously smaller than other stations by about 1.5 s. Events from similar paths confirm these observations [*Song and Helmberger*, 1993a]. It appears that the anomaly comes from lateral variations in the lowermost mantle underneath the mid-Pacific, a well-known complex structure as reported by *Su et al.* [1994] and others. Note also there are some systematic discrepancies between the observed waveforms and synthetics in that the synthetics have a peak for *PKIKP* which seems sharper in distance range 150° to 156° and then broader beyond that. This might suggest an adjustment of the Q_α model. Alternatively, it might suggest some anom-

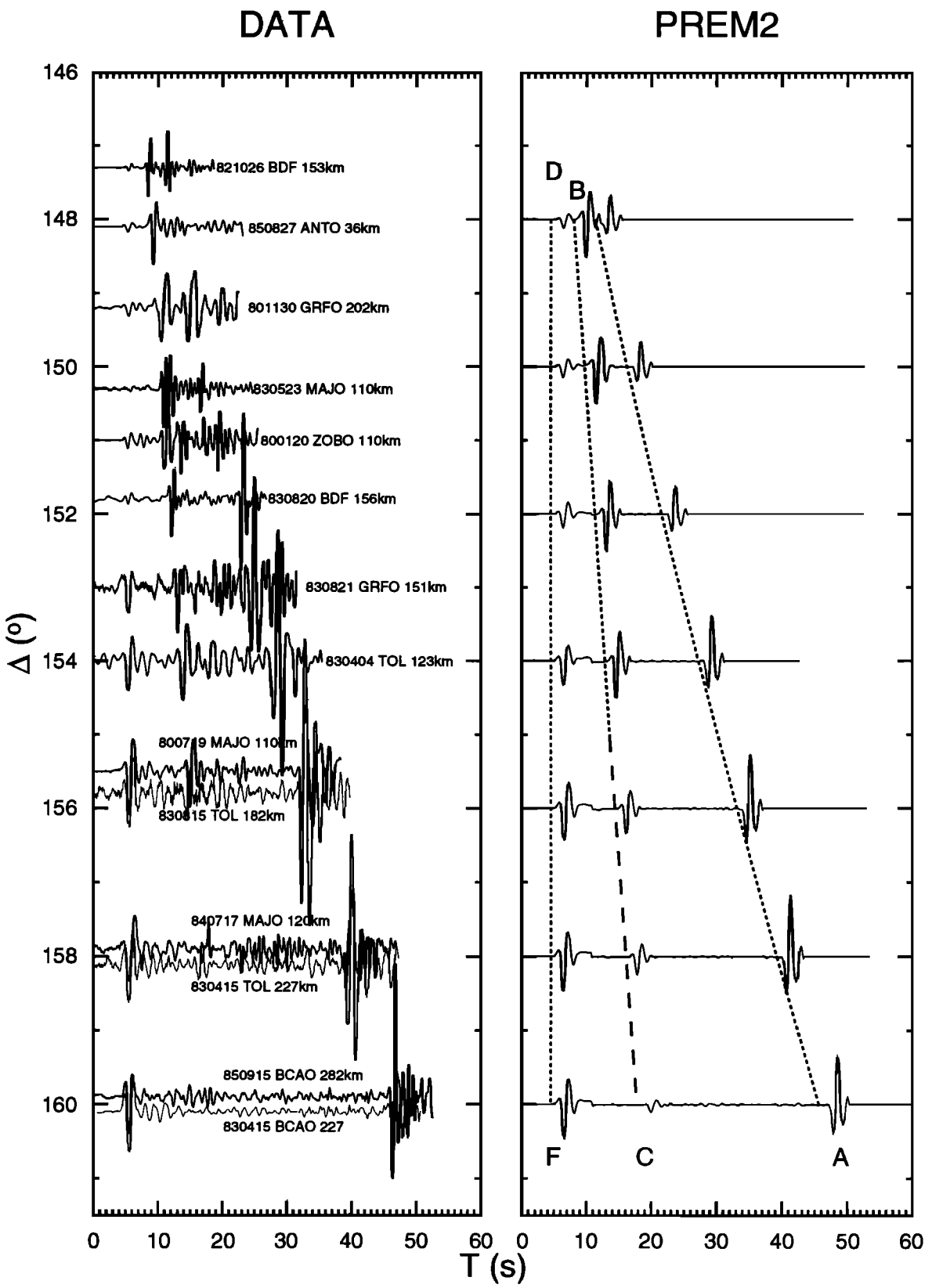

Figure 9. (left) A combined short-period GDSN record section from various events with focal depths around 150 km. The event dates, depths, and station names are printed near the records. (right) Synthetics for model PREM2 for a depth of 150 km except for the last trace at 160°, which is computed for a depth of 250 km.

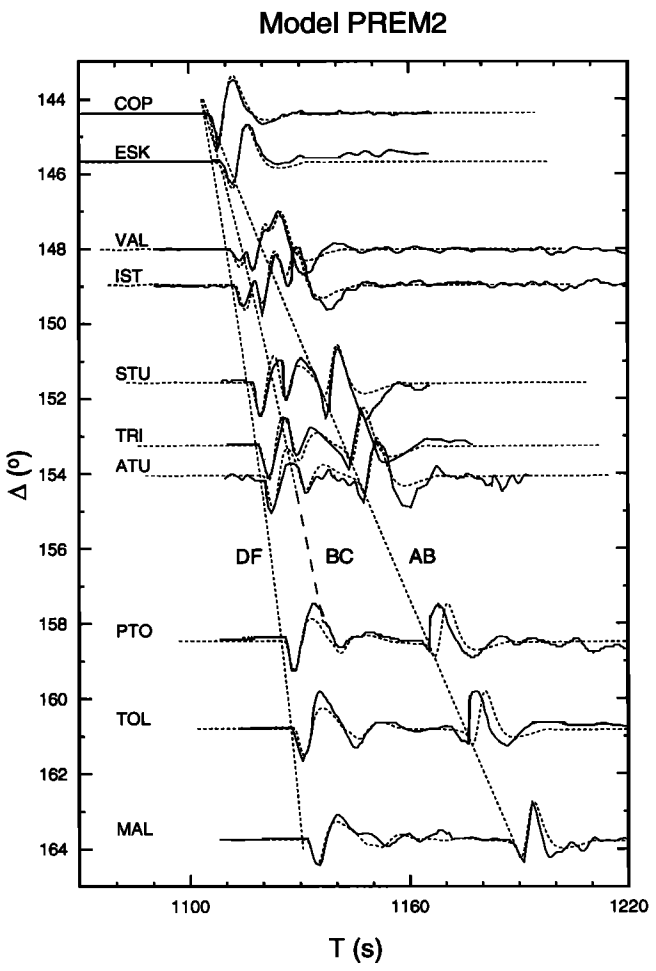

Figure 10. Comparisons of long-period records (solid) from the March 17, 1966, western Tonga event (h=627 km) with synthetics for PREM2 (dashed).

alous structure is affecting the observed waveforms, by noting that the relative amplitudes of *DF* and *AB* at PTO and TOL seem anomalous, in addition to anomalous differential times.

The fits of PREM synthetics to this same record section are presented in Figure 11. The time function used is the same as for the PREM2 synthetics. The $AB - DF$ times from the PREM synthetics agree better with those of the PTO and TOL. On the other hand, the $AB - DF$ times are smaller than those of all other stations except the stations approaching the *B*-caustic (COP, ESK, VAL), where the individual *PKP* arrivals become less discernible.

The above shifts of *AB* and *DF* differential travel times are quite common for long-period records worldwide. However, much more data sampling and waveform modeling are required to map the details of these anomalous structures. For this purpose, broadband modeling has particular advantages since shorter wavelengths are involved and better resolution can be obtained. The broadband data provided by the new digital systems are ideal, but not many records presently exist, especially on a global scale. Thus working with the combined short- and long-period WWSSN observations from the same event is motivated. An example of such data from an event occurring beneath Java (March 19, 1967; focal depth of 89 km) is displayed in Figure 12 along with the PREM2 synthetics. A t^*=0.35 s is applied to the *DF* branch of the synthetics. The time function is a trapezoid of (0.3 s, 0.3 s, 0.3 s). The data are shifted to line up with *BC* arrivals and normalized to peak-to-peak amplitudes. Note that records from station BEC (marked in thinner lines) have been shifted 2° to a larger distance to distinguish traces from LPB at the neighboring distance. The fits for short-period records are excellent in *PKIKP* (*DF*), *PKiKP* (*CD*), and *BC* waveforms. The *PKIKP* and *PKiKP* arrivals are distinctly observed in the short-period records between 130° and 140° and are correctly modeled by PREM2. The agreement suggests the average model (PREM2) provides a good representation for the velocity and attenuation structure from the bottom 400 km of the outer core to the top 400 km of the inner core where these paths sample beneath the central Pacific. The fits for *AB* arrivals vary, however. For example, *AB* arrivals are slightly earlier at ARE and much later at BOG (by 1.5 s) than the synthetics. The fits for the long-period record sections (right panel in Figure 12)

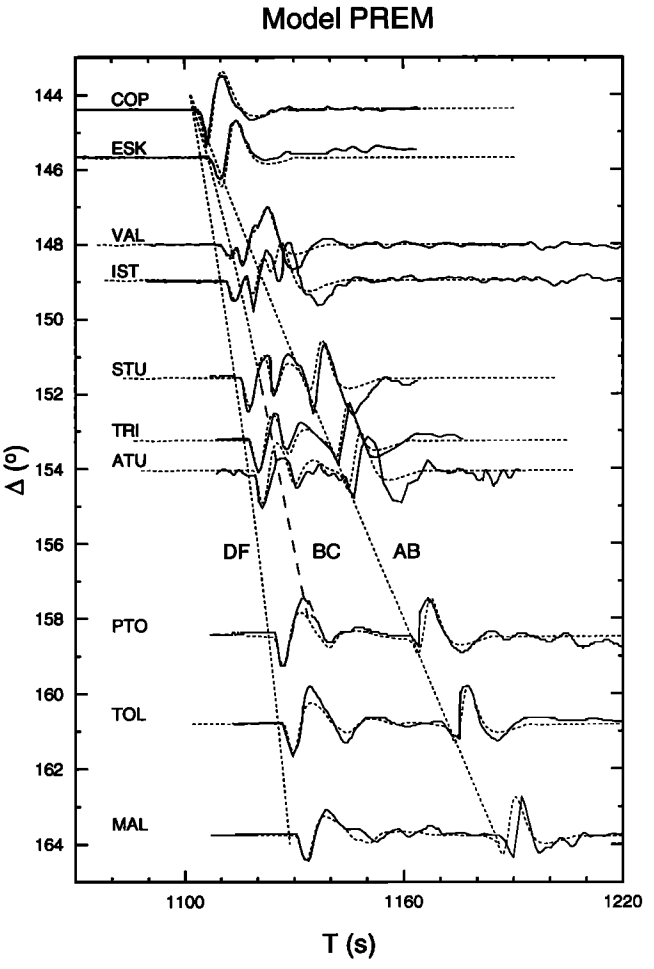

Figure 11. Comparisons of the long-period records from the Tonga event (solid) and synthetics for PREM (dashed).

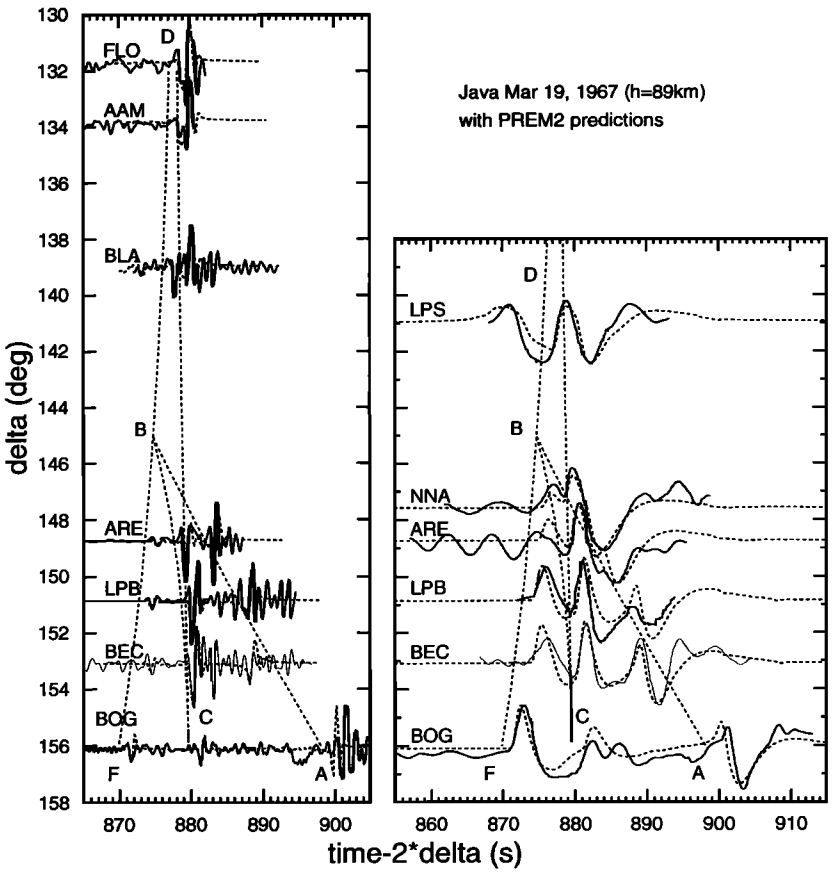

Figure 12. Comparisons of observations (solid) from the March 19, 1967, Java event (h=89 km) with synthetics for PREM2 (dashed) for short-period and long-period WWSSN instruments. The BEC records (light lines) are shifted down 2° for better reading.

are less impressive. The data are not of the best quality as the noise level is high. However, *AB* arrivals are clearly late by about 1.0 s at BOG. The variations of the *AB* phase in timing and in amplitudes displayed in these records have been observed in bigger data sets of $AB - DF$ and DF/AB and have been interpreted as the influence of lateral heterogeneity in the lowermost mantle [*Sacks et al.*, 1979; *Song and Helmberger*, 1993a], pointed out earlier in the text.

The comparisons of the synthetics for PREM and the short-period records for the above Java event are displayed in Figure 13. The time function used is the same as for the PREM2 synthetics. The synthetics on the left are calculated assuming a constant $t^*=0.35$ s for the inner core attenuation and those on the right are for a constant $Q_\alpha=333$. The PREM synthetics on the left fit the *DF* and *BC* waveforms fairly well between 148° and 153°. However, discrepancies are obvious in other distance ranges. The separation between *PKIKP* (*DF*) and *PKiKP* (*CD*) in the synthetics is clearly smaller than those of the observations between 132° and 140°, suggesting that a larger P velocity increase than PREM is required at the ICB. The $PKP\text{-}C_{diff}-DF$ times from the PREM synthetics are smaller (by about 0.3 s) than that of the observation at BOG near 156°. The predicted amplitude of $PKP\text{-}C_{diff}$ is also too small relative to those of *DF* and *AB* compared with the observation. The predicted amplitude of $PKP\text{-}C_{diff}$ at BOG for a constant Q_α, on the right, still appears too small relative to that of *DF* even though the *DF* arrival is more attenuated with this Q_α model (equivalent $t^*=0.47$ s at this distance). Thus the relative timing and amplitude of the *DF* and $PKP\text{-}C_{diff}$ arrivals at BOG are consistent with a velocity reduction at the bottom of the outer core from PREM. Note that amplitudes *PKIKP* (*DF*) of the synthetics at ranges from 132° to 140° on the right are too large compared with the data, favoring a higher attenuation at the top of the inner core (or a smaller Q_α value than 333).

Concluding Remarks

Resolving the detailed seismic properties of the core remains integral in understanding the dynamics of Earth. This is especially true at the CMB and ICB, where the structure near the boundary layers provides constraints on composition and thermal state. In this study we have presented our best 1-D structure to assist other scientists in their quest for meaningful physical models and as a reference in comparing other seismological data.

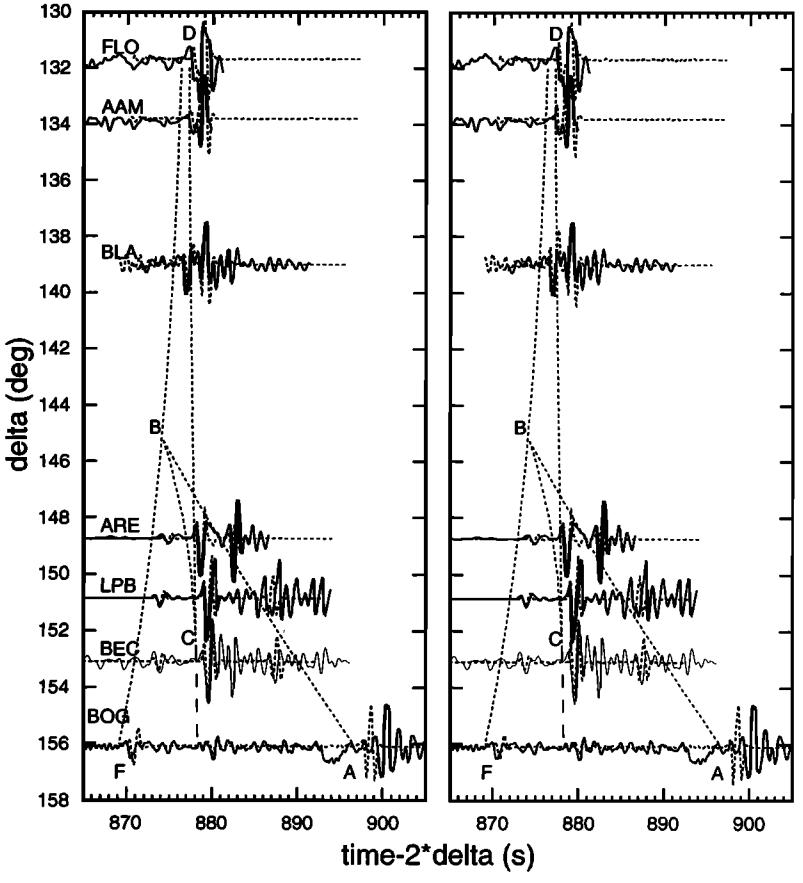

Figure 13. Comparisons of the short-period records from the Java event (solid) and synthetics for PREM (dashed) for two attenuation models of the inner core: (left) constant t^*=0.35 s; (right) constant Q_α=333. Note that the PREM synthetics do not fit observations in the range of 132° to 140° and at station BOG for both cases.

Since PREM has proven quite effective in other studies, we have attempted to keep most of its structure intact. For example, *Garnero et al.* [1993a] recently discovered that multiple *SmKS* waves for m=2, 3, 4 are commonly observed at large ranges, where $m-1$ denotes the number of times this phase reflects beneath the CMB. The timing between these multiples provides an excellent tool for determining the upper part of the outer core velocity structure. Predictions of PREM generally fit well both in timing and in waveform. However, PREM does appear too fast in the lowermost mantle, D'', as demonstrated recently by *Song and Helmberger* [1993a]. Thus the separation between the *PKP* phases, $AB-DF$, is about 2 s too small at ranges greater than 150°. However, there is increasing evidence showing that the lowermost mantle is laterally varying for both *S* wave and *P* wave structure, the latest works of which include those of *Wysession et al.* [1992], *Kendall and Shearer* [1994], and others. All the core phases are subject to such variations, with $AB-DF$ times of *PKP* being affected the most and $BC-DF$ as well as (*PKIKP*+*PKiKP*) waveforms being affected the least in our case. Such an impact of the lowermost mantle structure on the *PKP* phases was investigated in our earlier systematic search of six years of the GDSN short-period data on CD-ROM [*Song and Helmberger*, 1993a]. Of a total 1898 records available for the distances of 147° to 165°, 47 high-quality records with cross-correlation coefficients of *DF* and *AB* (Hilbert-transformed) greater than 0.5 were selected. Why these phases are so incoherent is not known. Nevertheless, this high rejection rate results in poor coverage of the lower mantle. However, the six sampled regions obtained show coherent geographical variations of up to 2 s in $AB-DF$ times. Fortunately, these travel time anomalies obtained from the short-period records agree with long-period records available from WWSSN. For example, paths from Fiji-Tonga events to TOL show smaller $AB-DF$ times by 0.5-2.0 s compared with other paths, compatible with the record section in Figure 10. Thus we are confident that the scatter in the $AB-DF$ times as in Figure 6 is real and not a result of random errors. The observed fast-slow patterns generally agree with the anomaly map of *Creager and Jordan* [1986] from a much larger data set of *AB* and *DF* arrival times as discussed in *Song and Helmberger* [1993a], although our observed variation is almost twice as large. The discrepancies of the observed anomalies from the body waves become more obvious when compared with other tomographic models of the lower most mantle as presented by *Song*

and Helmberger [1993c] and will be reported in a future paper.

In the light of this regional variation, we emphasize once again that our modification in the lowermost mantle is the average of our limited samples and is subject to change with better sampling. On the other hand for practical purposes, such modification can serve as baseline adjustments for $AB - DF$ differential travel time predictions of the PREM model. The adjustments for PREM predictions range from 0.4 s at 148° to 1.3 s at 164° for a surface focus. Although they are still subject to verification from larger data sets and more grazing AB arrivals at greater distances, such adjustments are useful in providing a reference for studying higher-resolution features of lateral variations in the lowermost mantle [*Song and Helmberger*, 1993a; *Creager and McSweeney*, 1993] and the anisotropy of the inner core [*Vinnik et al.*, 1994] using $AB - DF$ measurements. If a global decrease in D'' velocities on average is true, the immediate implication would be that there must be D'' regions with very slow velocities to balance high-velocity regions reported in the literature [*Lay and Helmberger*, 1983; *Young and Lay*, 1990; *Gaherty and Lay*, 1992; *Kendall and Shearer*, 1994; *Baumgardt*, 1989; *Revenaugh and Jordan*, 1991; *Vidale and Benz*, 1993; *Weber and Davis*, 1990; *Krüger et al.*, 1993; *Wysession et al.*, 1992]. The major issues of these studies were the D'' lateral heterogeneities and its discontinuities where the baselines or the absolute values of reference models were of no concern. One of these studies that involves P velocity by *Wysession et al.* [1992] does support a reduced P velocity in D'' from PREM. Of total 11 samples of P_{diff}, eight regions show slower average velocities than that of PREM. The scale bar ranges from -2.0% (slow) to +1.0% (fast) relative to PREM with the average center at -0.5% (slow). A very slow anomaly of -3.2% was identified from Tonga to Mid-East, sampling CMB under northern Indonesia, while the fastest anomaly found was only 0.8%. The possible existence of low P velocities at the base of the mantle was suggested by *Garnero et al.* [1993b] from SKS and SP_dKS waveform modeling. This result if proved on a global scale would have profound implications on the structure and composition at the CMB and is being rigorously pursued.

The major changes to PREM occur near the ICB, where adjustments were made to satisfy the waveform data and differential timing. The ICB remains sharp but with a larger velocity jump. Our choice of the jump of 0.78 km/s, which falls between that of PREM (0.68 km/s) and that of PEM (0.83 km/s) [*Song and Helmberger*, 1992], is tightly constrained (within an uncertainty of ±0.02 km/s) by modeling a short-period LRSM record section and a short-period WWSSN record section, sampling the ICB under the northeastern Pacific. However, similar studies are required for other paths to investigate possible lateral variations, as suggested by *Kaneshima et al.* [1994]. The most noticeable change occurs at the bottom of the outer core where the velocity gradient is reduced to near zero. This low gradient persists over the lowermost 150 km and produces satisfactory fits to our $BC - DF$ differential travel times. This model fits the BC times of *Souriau and Poupinet* [1991] as well as the BC and $BC - DF$ times of E. R. Engdahl (personal communications, 1994) from ISC. This small velocity gradient in the lowermost outer core has also been found in regional studies of PKP phases [e.g., *Müller*, 1973; *Qamar*, 1973; *Song and Helmberger*, 1992]. A recent study by *Kaneshima et al.* [1994] also suggests a reduction of the velocity gradient at the bottom of the outer core from PREM based on a broadband record at the range of 152.4°, although the reduction is not as pronounced as in the studies above or in this study. In our previous model PMNA of the ICB [*Song and Helmberger*, 1992], a small velocity gradient over the lower 400 km of the outer core was used to model the waveforms of the long-period diffraction from PKP B-caustic. The structure, however, is much broader than here in PREM2. The discrepancy is possibly due to path variations, limited resolution of long-period data, and possible complication from the double-source mechanism (unfortunately) as well as the trade-off between the middle outer core and the lower outer core not explored in this study.

One difficulty of having a very low velocity gradient in this region is that it predicts a relatively strong PKP-C_{diff} beyond the C-cusp [*Choy and Cormier*, 1983], which is not always observed. Because of the high sensitivities of these diffracted waves to the gradient, it is possible to adjust the velocity gradient in the very bottom of the outer core and in the neighboring region above to model these diffracted waves as we successfully demonstrated above. Further constraints on this velocity structure and possible lateral variations will come from modeling regional broadband seismic data.

It is important to realize that the determination of this velocity gradient has been crucial in the derivation of density stratification and the physics of Earth's core. From *Bullen* [1963], the Bullen parameter of radial inhomogeneity is defined by

$$\eta = \frac{dK}{dP} + g^{-1}\frac{d\Phi}{dr} \tag{1}$$

where dK/dP is the pressure derivative of bulk modulus and $\Phi = V_p^2 - 4/3V_s^2$ is the seismic parameter. Both terms are physically measurable and can be determined independently. A value of η equal to unity implies uniform chemical composition. With the second term in (1) vanishing, $\eta \approx dK/dP$. With dK/dP slowly varying around 3.5 at the outer core pressure from a recent work by *Anderson and Ahrens* [1994] on an equation of state for liquid iron based on experimental data, the inhomogeneity at the bottom of the outer core is "practically inescapable" as is the case for D'' pointed out by *Bullen* [1963] three decades ago.

Acknowledgments. We thank Eddie Garnero and Don Anderson for helpful comments, Bill Anderson and Tom Ahrens for discussions on equation of state for liquid iron, and Bob Engdahl for testing the PREM2 model and helpful discussions. The critical reviews and useful comments from Phil Cummins, Associate Editor Michael Wysession, and Bob Engdahl greatly improved the manuscript, for which

we are thankful. This research was supported by National Science Foundation grant EAR-89-04767. This is Division of Geological and Planetary Sciences, California Institute of Technology, contribution 5375.

References

Anderson, W.W., and T.J. Ahrens, An equation of state for liquid iron and implications for the Earth's core, *J. Geophys. Res.*, *99*, 4273-4284, 1994.

Baumgardt, D.R., Evidence for a *P* wave velocity anomaly in *D''*, *Geophys. Res. Lett.*, *16*, 657-660, 1989.

Bhattacharyya, J., P.M. Shearer, and G. Masters, Inner-core attenuation from short-period *PKP(BC)* versus *PKP(DF)* wave-forms, *Geophys. J. Int.*, *114*, 1-11, 1993.

Bullen, K.E., An index of degree of chemical inhomogeneity in the Earth, *Geophys. J.*, *7*, 584-592, 1963.

Choy, G.L., and V.F. Cormier, The structure of the inner core inferred from short-period and broadband GDSN data, *Geophys. J. R. Astron. Soc.*, *72*, 1-21, 1983.

Cormier, V.F., Short-period *PKP* phases and the anelastic mechanism of the inner core, *Phys. Earth Planet. Inter.*, *24*, 291-301, 1981.

Creager, K.C., Anisotropy of the inner core from differential travel times of the phases *PKP* and *PKIKP*, *Nature*, *356*, 309-314, 1992.

Creager, K. C., and T. H. Jordan, Aspherical structure of the core-mantle boundary from *PKP* travel times, *Geophys. Res. Lett.*, *13*, 1497-1500, 1986.

Creager, K.C., and T.J. McSweeney, Length scales of mantle dregs from *PKP* observations, *Eos Trans. AGU*, *74(43)*, Fall Meeting Suppl., 416, 1993.

Cummins, P., and L. Johnson, Short-period body wave constraints on properties of the Earth's inner core boundary, *J. Geophys. Res.*, *93*, 9058-9074, 1988.

Doornbos, D.J., The anelasticity of the inner core, *Geophys. J. R. Astron. Soc.*, *38*, 397-415, 1974.

Dziewonski, A.M., and D.L. Anderson, Preliminary reference Earth model, *Phys. Earth Planet. Inter.*, *25*, 297-356, 1981.

Dziewonski, A.M., A.L. Hales, and E.R. Lapwood, Parametrically simple earth models consistent with geophysical data, *Phys. Earth Planet. Inter.*, *10*, 12-48, 1975.

Gaherty, J.B., and T. Lay, Investigation of laterally heterogeneous shear velocity structure in *D''* beneath Eurasia, *J. Geophys. Res.*, *97*, 417-435, 1992.

Garnero, E., D. V. Helmberger, and S.P. Grand, Constraining outermost core velocity with *SmKS* waves, *Geophys. Res. Lett.*, *20*, 2463-2466, 1993a.

Garnero, E., S.P. Grand, and D.V. Helmberger, Low *P* wave velocity at the base of the mantle, *Geophys. Res. Lett.*, *20*, 1843-1846, 1993b.

Kaneshima, S., K. Hirahara, T. Ohtaki, and Y. Yoshida, Seismic structure near the inner core-outer core boundary, *Geophys. Res. Lett.*, *21*, 157-160, 1994.

Kendall, J.M., and P.M. Shearer, Lateral variations in *D''* thickness from long-period shear-wave data, *J. Geophys. Res.*, *99*, 11575-11590, 1994.

Kennett, B.L.N., and E.R. Engdahl, Traveltimes for global earthquake location and phase identification, *Geophys. J. Int.*, *105*, 429-465, 1991.

Krüger, F., M. Weber, and F. Scherbaum, Double-beam analysis of anomalies in the core-mantle boundary region, *Geophys. Res. Lett.*, *20*, 1475-1478, 1993.

Lay, T., and D.V. Helmberger, A lower mantle *S* wave triplication and the shear velocity structure of *D''*, *Geophys. J. R. Astron. Soc.*, *75*, 799-837, 1983.

Morelli, A., and A.M. Dziewonski, Body wave traveltimes and a spherically symmetric *P* and *S* wave velocity model, *Geophys. J. Int.*, *112*, 178-194, 1993.

Mortenson, M.E., *Geometric Modeling*, pp. 113-125, John Wiley, New York, 1985.

Müller, G., Amplitude studies of core phases, *J. Geophys. Res.*, *78*, 3469-3490, 1973.

Qamar, A., Revised velocities in the Earth's core, *Bull. Seismol. Soc. Am.*, *63*, 1073-1105, 1973.

Revenaugh, J., and T.H. Jordan, Mantle layering from *ScS* reverberations, 4, The lower mantle and core-mantle boundary, *J. Geophys. Res.*, *96*, 19811-19824, 1991.

Sacks, I.S., and J.A. Snoke, and L. Beach, Lateral heterogeneity at the base of the mantle revealed by observations of amplitudes of *PKP* phases, *Geophys. J. R. Astron. Soc.*, *59*, 379-387, 1979.

Shearer, P.M., and K.M. Toy, *PKP(BC)* versus *PKP(DF)* differential travel times and aspherical structure in the Earth's inner core, *J. Geophys. Res.*, *96*, 2233-2247, 1991.

Song, X.D., and D.V. Helmberger, Velocity structure near the inner core boundary from waveform modeling, *J. Geophys. Res.*, *97*, 6573-6586, 1992.

Song, X.D., and D.V. Helmberger, Effect of velocity structure in *D''* on *PKP* phases *Geophys. Res. Lett.*, *20*, 285-288, 1993a.

Song, X.D., and D.V. Helmberger, Anisotropy of Earth's inner core, *Geophys. Res. Lett.*, *20*, 2591-2594, 1993b.

Song, X.D., and D.V. Helmberger, Lateral variations of lower mantle structure, *Eos Trans. AGU*, *74(16)*, Spring Meeting Suppl., 213, 1993c.

Souriau, A., and G. Poupinet, The velocity profile at the base of the liquid core from *PKP(BC+C$_{diff}$)* data: An argument in favor of radial inhomogeneity, *Geophys. Res. Lett.*, *18*, 2023-2026, 1991.

Su, W.J., R.L. Woodward, and A.M. Dziewonski, Degree 12 model of shear velocity heterogeneity in the mantle, *J. Geophys. Res.*, *99*, 6945-6980, 1994.

Tromp, J., Support for anisotropy of the Earth's inner core from free oscillations, *Nature*, *366*, 678-681, 1993.

Vidale, J.E., and H.M. Benz, Seismological mapping of fine-structure near the base of the Earth's mantle, *Nature*, *361*, 529-532, 1993.

Vinnik, L., B. Romanowicz, and L. Breger, Anisotropy in the inner core from the broadband records of the geoscope network, *Geophys. Res. Lett.*, *21*, 1671-1674, 1994.

Weber, M., and J.P. Davis, Evidence of a laterally variable lower mantle structure from *P* waves and *S* waves, *Geophys. J. Int.*, *102*, 231 -255, 1990.

Wysession, M.E., E.A. Okal, and C.R. Bina, The structure of the core-mantle boundary from diffracted waves, *J. Geophys. Res.*, *97*, 8749-8764, 1992.

Young, C.J., and T. Lay, Multiple phase analysis of the shear velocity structure in the *D''* region beneath Alaska, *J. Geophys. Res.*, *95*, 17,385-17,402, 1990.

D. V. Helmberger, Seismological Laboratory, California Institute of Technology, Pasadena, CA 91125. (email: helm@seismo.gps.caltech.edu)

X. D. Song, Lamont-Doherty Earth Observatory of Columbia University, Palisades, NY 10964. (email: xsong@ldeo.columbia.edu)

(Received February 3, 1994; revised October 31, 1994; accepted November 29, 1994.)